

Real-time study of nucleation, growth, and ripening during Fe/Fe(100) homoepitaxy using ion scattering

R. Pfandzelter,* T. Igel, and H. Winter

Humboldt-Universität zu Berlin, Institut für Physik, Invalidenstrasse 110, 10115 Berlin, Germany

(Received 15 May 2000)

Real-time studies of submonolayer epitaxy via scattering of fast ions are applicable over a wide range of growth temperatures and deposition rates. Computer simulations of ion trajectories and nucleation theory yield quantitative information on atomistic growth processes. For homoepitaxy of Fe on Fe(100), we deduce island densities, monomer diffusion barrier, cluster binding energies, and post-deposition island ripening. Detailed information on transitions in critical cluster size is obtained.

Understanding the physics of epitaxial growth on crystal surfaces is fundamental for the production of thin films. Although the basic atomic processes involved are conceptually simple, the far-from-equilibrium dynamics of growth requires quantitative knowledge on all competing kinetic and energetic parameters for reliable predictions on film morphologies. Therefore, experimental studies are indispensable, preferably by using techniques working *in situ* and in real time. In addition, the technique should be applicable over a wide range of growth temperatures and deposition rates. In fact, by tuning temperature and rate, one can produce very different film morphologies, depending on the kinetic limitations in force.

In epitaxial growth of submonolayer films on flat single crystal surfaces, atoms from an impinging beam arrive at random positions on the substrate surface and begin to migrate. Diffusing adatoms, or monomers, may meet further adatoms and form nuclei. These nuclei dissociate before other adatoms join them or form stable islands. The density of these islands increases until the island separation becomes comparable to the adatom diffusion length. Then, most adatoms attach to islands inhibiting further significant nucleation, i.e., the density of nucleated islands saturates. Island growth continues until islands come into contact with each other, resulting in coalescence. This scenario of diffusion, nucleation, aggregation, and coalescence is fundamental for submonolayer growth, though details are system specific.

The saturation island density N is controlled by the experimental parameters substrate temperature T and deposition rate F . For two-dimensional (2D) islands and complete condensation on isotropic substrates, nucleation theory yields the scaling law¹

$$N = \eta \left(\frac{D}{F} \right)^{-i/(i+2)} \exp \left(\frac{E_i/kT}{i+2} \right), \quad (1)$$

where $D = 1/4\nu_0 \exp(-E_d/kT)$ is the tracer diffusion coefficient with attempt frequency ν_0 and diffusion barrier E_d . i denotes the critical cluster size corresponding to $(i+1)$ atoms needed to form the smallest stable island. E_i is the lateral binding energy of the critical cluster ($E_1=0$), which is given, in a simple approximation, by the number of nearest-neighbor adatom bonds times a bond energy E_b (pair-binding model). k is the Boltzmann constant and $\eta \approx 0.2$.² In the case

of irreversible nucleation with stable dimers ($i=1$), E_d and ν_0 can be deduced from measured island densities N in an Arrhenius plot,³ and i from log-log plots of the island density versus deposition flux.

In this paper, we demonstrate that these key quantities in submonolayer epitaxy can be obtained from grazing-angle scattering of fast ions. We report on a systematic study of homoepitaxial growth of Fe on Fe(100), where the intensity of specularly reflected ions is measured during and after deposition over a wide range of temperatures and deposition rates. A quantitative analysis of data based on computer simulations emulating ion trajectories and nucleation theory [Eq. (1)] yields information on diffusion barrier, cluster binding energies, and post-deposition behavior. Our results resolve a controversy on transitions in critical cluster size.

Fe on Fe(100) is considered as a model system in metal epitaxy since a seminal scanning tunneling microscopy (STM) study of Stroscio *et al.*⁴ Those authors deposited submonolayer amounts at elevated temperatures and performed STM measurements at room temperature. With $i=1$, they inferred from an Arrhenius dependence of the island density on temperature for $T < 520$ K a diffusion barrier $E_d = 0.45$ eV. Inspection of the distribution of island sizes corroborated that nucleation is irreversible in this temperature range.⁵ For higher temperatures, smaller island densities with narrower size distributions indicated a change in critical cluster size. Tentatively, $i=3$ has been suggested.

Although stable tetramers are plausible from bond-counting arguments, the possibility of a well-defined $i=3$ regime has been discussed in a number of subsequent theoretical studies, mainly based on kinetic Monte Carlo simulations.^{6,7,8} In fact, extended transition regimes have been proposed, where i changes between integer or even noninteger values, indicating that i should be considered an effective quantity owing to a statistical average over different cluster sizes. For a clarification of these issues, measurements of island densities over a wide range of deposition flux are required.

Unprecedented information on submonolayer epitaxial growth has been obtained by direct imaging using STM.³ Despite the benefits of STM owing to a unique resolution, problems may arise for imaging during growth, especially at elevated temperatures, and because of slow imaging rates.

Indirect techniques working in reciprocal space, such as diffraction of high (RHEED) or low (LEED) energy electrons^{4,9,10} or thermal-energy atoms,¹¹ stand out for their superior statistics. Quantitative information has been extracted from an analysis of angular profiles of diffraction beams. As an alternative to diffraction techniques, grazing scattering of keV ions from the film surface has been introduced as a real-space technique.¹² Based on a classical picture, trajectories of ions are determined by a series of small-angle deflections, leading to specular reflection. Growth-induced defects like adatoms or step-edges of islands perturb the correlated scattering process resulting in a loss of the specular-beam intensity. Interpretation is straightforward and based on classical mechanics computer simulations.¹³ As will be shown, there are virtually no restrictions concerning growth temperature or deposition rate.

Our experimental setup is described in Ref. 14. In brief, a well collimated beam of 25 keV He⁺ ions is directed upon a clean and flat (mean terrace width > 2000 Å) Fe(100) surface at a grazing polar angle $\Phi_{in} = 1.75^\circ$ with respect to the surface plane and an azimuthal angle of a few degrees to the [001] surface lattice direction. Specularly reflected projectiles ($\Phi_{out} \approx \Phi_{in}$) are recorded by means of a channeltron detector with small angular acceptance ($\pm 0.02^\circ$). Fe is deposited from a high-purity wire by electron beam heating. During growth, the background pressure does not exceed 1×10^{-10} mbar. The target temperature is measured by a thermocouple with ± 10 K and held constant during growth to ± 1 K.

Figure 1 shows the specular-beam intensity recorded during growth of about 1 monolayer (ML) at different temperatures and deposition rates. The oscillatory behavior is well-known from diffraction techniques and reflects the periodic change in surface morphology. In the simulations (curves) ions are scattered from 2D pseudomorphic islands on a semi-infinite Fe(100) crystal. The average separation between islands is assumed to be independent of coverage (constant island density). The distributions of island sizes and separations are described by gamma distributions with two parameters α for the average value, and M for the shape of the distribution function.¹³ The adequacy of a gamma distribution with $M \approx 2-3$ has been inferred from LEED studies^{10,15} and, for Fe(100) homoepitaxy, an evaluation of STM images¹³ and Monte Carlo simulation results.⁷

The curves in Fig. 1 represent fits with fitparameter α and $M=3$ to measured intensities around the minimum, where the island density is saturated and about constant (aggregation regime).¹⁶ The model is less adequate at low coverages owing to a rapid increase in island density (nucleation regime) and, at the very beginning of deposition, migrating adatoms. Discrepancies upon approaching monolayer coverage are ascribed to coalescence and nucleation and growth on top of islands.

The simulation describes the observed behavior quite well in a range of coverages from about 0.2–0.6 ML. This corresponds to coverages where characteristic side bands appear in electron and atom diffraction patterns, reflecting constant average island separations.^{9,10,11} Although this coverage range already extends into the coalescence regime, Bartelt and Evans¹⁶ pointed out that, in the absence of a complete restructuring upon coalescence, diffraction theory should be

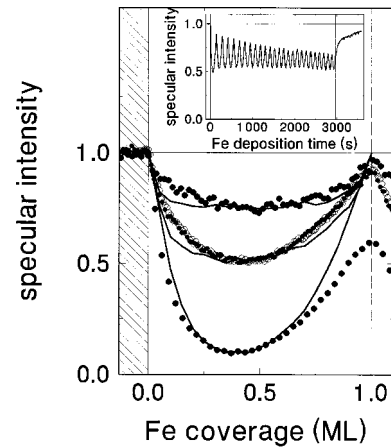


FIG. 1. Measured (circles) and simulated (curves) intensity (normalized) of specularly reflected 25 keV He⁺ ions during homoepitaxial growth on Fe(100). Growth temperatures (from top to bottom): 590, 590, and 420 K; deposition rates: 9.0×10^{-3} , 5.8×10^{-2} , and 2.1×10^{-1} ML s⁻¹ (a further run marked by open circles shows the reproducibility). The simulations are best fits (islands densities: 1.74×10^{10} , 9.47×10^{10} , and 2.37×10^{12} cm⁻²). Inset: Specular-beam intensity at 550 K, showing that growth proceeds in a nearly perfect layer-by-layer mode.

formulated in terms of *nucleated* islands rather than *actual* islands. This applies also for ion scattering, considering the large step-edge lengths of ramified clusters of coalesced islands.

The temperature dependence of the saturation island density is shown in Fig. 2 (solid circles) together with the STM data from Stroscio *et al.*⁴ (open squares) for the same deposition rate. We find good agreement for not too high temperatures. From a linear fit to the data for $T \leq 470$ K we deduce from Eq. (1) $E_d = (0.485 \pm 0.050)$ eV and $v_0 = 9$

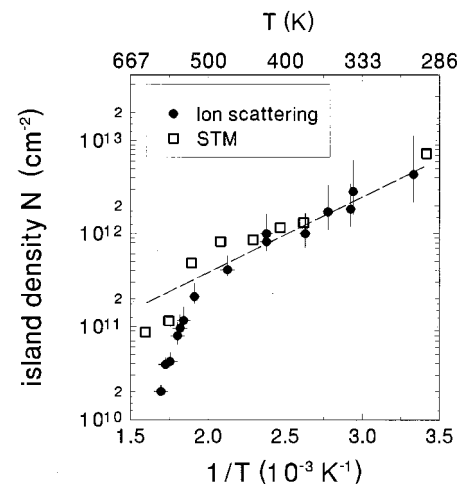


FIG. 2. Arrhenius plot of saturation island densities obtained from the intensity of reflected ions (solid circles). The line is a fit to the data for $T \leq 470$ K. The deposition rate was $(1.15 \pm 0.4) \times 10^{-2}$ ML s⁻¹. The error bars include uncertainties in experiment and simulation (insufficient knowledge of island size distribution, correction for the nominal rate according to Fig. 3). Open squares show STM results from Stroscio *et al.* (Ref. 4) for the same deposition rate.

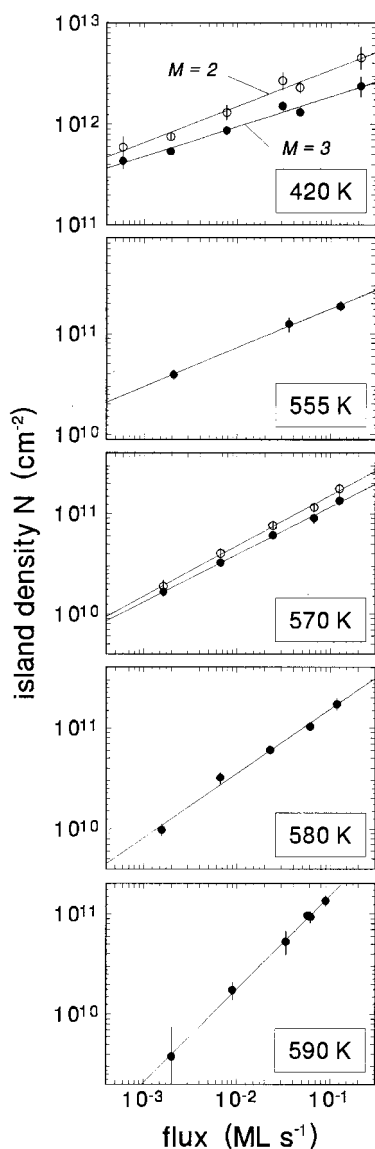


FIG. 3. Saturation island densities versus deposition flux obtained from the intensity of reflected ions during growth at temperatures as indicated. Open and solid circles correspond to island size distributions parametrized by $M=2$ and $M=3$, respectively.

$\times 10^{11 \pm 0.7} \text{ s}^{-1}$ for single adatom diffusion. Above 470 K, a pronounced decrease in island density is observed with systematic differences to STM data. Possible reasons are temperature calibration, time effects (temperature quenching in Ref. 4) or, for the smallest densities, effects owing to finite substrate terrace widths.

The implicit assumption of irreversible nucleation ($i=1$) at low temperatures is corroborated by log-log plots of the island density versus deposition flux, measured at constant temperature (Fig. 3). For $T=420$ K, a linear fit to the data over almost three decades in F (solid circles) yields $i=(0.84 \pm 0.09)$. The use of $M=2$ in the simulations, which corresponds to broader island size distributions,^{13,7} yields $i=(1.12 \pm 0.13)$ (open circles).

Our data show a linear dependence for $\log N$ versus $\log F$ even for high temperatures (Fig. 3), but with larger slopes. This clearly demonstrates an increase in the critical cluster size i . From linear fits we deduce $i=(1.25 \pm 0.11)$ at 555 K,

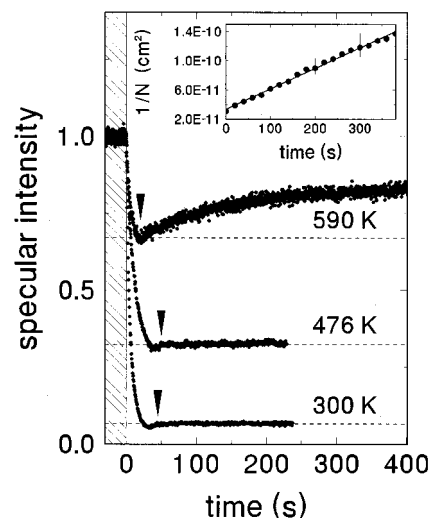


FIG. 4. Intensity of reflected ions (normalized) versus time for growth temperatures as indicated. The shutter was opened at $t=0$ (vertical line) and closed at a coverage of 0.5 ML (arrows). Inset: Reciprocal saturation island density versus time after closing the shutter as obtained from the 590 K curve.

(1.80 ± 0.09) at 570 K [$i=(2.02 \pm 0.12)$ for $M=2$], (3.54 ± 0.48) at 580 K, and (29 ± 9) at 590 K. These results do not support the assumption of a well-defined $i=3$ regime. The critical cluster size rather increases with increasing temperature with noninteger i . Considering the uncertainty in M , it cannot be excluded that the system switches between integer values.

Equation (1) can be used to estimate the binding energies of critical clusters E_i from the intercepts of lines in Fig. 3. Using E_d and v_0 derived above, we deduce for $i \approx 2$ at 570 K, $E_2=(0.38 \pm 0.15)$ eV. For $i \approx 3$ at 580 K, $E_3=(1.00 \pm 0.23)$ eV, in good agreement with 1.1 eV suggested in Ref. 5. Adopting the pair-binding model, it seems that the bond energy $E_b=0.5$ eV in the trimer is larger than in the dimer.⁸

In addition, grazing ion-surface scattering allows one to monitor the evolution of film morphologies immediately after deposition. Apart from studies of 3D smoothening, post-deposition behavior has been addressed with respect to ripening and dissolution of 2D islands.^{17,18,19,20} In Fig. 4 we show the intensity of reflected ions recorded during and after deposition for fixed temperature. For temperatures where nucleation is irreversible, the signal remains constant when the shutter is closed at 0.5 ML (arrows in Fig. 4). This indicates the absence of recovery effects during the time interval studied. At high temperatures an increase in the specular-beam intensity shows that the saturated island density N decreases with time after deposition. Data evaluation yields $N \propto t^{-1}$ (Fig. 4, inset). This is in accordance with Ostwald ripening of small 2D islands kinetically limited by attachment and detachment,¹⁹ in contrast to the $t^{-2/3}$ dependence expected when diffusion between islands is the rate-limiting process.

In conclusion, we have shown that grazing ion-surface scattering can be used to quantitatively study nucleation, growth, and ripening processes in submonolayer epitaxy. A straightforward analysis based on classical mechanics com-

puter simulations and nucleation theory links the specular-beam intensity to atomistic quantities like diffusion barriers or binding energies. The method is complementary to established techniques, like STM or electron diffraction, as it works in real-time and real-space at virtually all growth temperatures and deposition rates. Application of the method to submonolayer growth of Fe on Fe(100) yields a comprehensive view of the temporal evolution of the film morphology

and its dependence on growth temperature and deposition rate. In particular, detailed information on transitions in critical cluster size are obtained.

We thank A. Laws, K. Maass, and R. A. Noack for their assistance in the preparation of the experiments. This work was supported by the Deutsche Forschungsgemeinschaft (Sonderforschungsbereich 290).

*Email address: pfandz@physik.hu-berlin.de FAX: +49 30 2093 7899.

¹J. A. Venables, *Philos. Mag.* **27**, 697 (1973); *Phys. Rev. B* **36**, 4153 (1987).

²J. A. Venables, G. D. T. Spiller, and M. Hanbücken, *Rep. Prog. Phys.* **47**, 399 (1984).

³H. Brune, *Surf. Sci. Rep.* **31**, 121 (1998), and references therein.

⁴J. A. Stroscio, D. T. Pierce, and R. A. Dragoset, *Phys. Rev. Lett.* **70**, 3615 (1993).

⁵J. A. Stroscio and D. T. Pierce, *Phys. Rev. B* **49**, 8522 (1994).

⁶C. Ratsch, A. Zangwill, P. Šmilauer, and D. D. Vvedensky, *Phys. Rev. Lett.* **72**, 3194 (1994); C. Ratsch, P. Šmilauer, A. Zangwill, and D. D. Vvedensky, *Surf. Sci. Lett.* **329**, L599 (1995).

⁷J. G. Amar and F. Family, *Phys. Rev. Lett.* **74**, 2066 (1995).

⁸M. C. Bartelt, L. S. Perkins, and J. W. Evans, *Surf. Sci. Lett.* **344**, L1193 (1995).

⁹J.-K. Zuo, J. F. Wendelken, H. Dürr, and C.-L. Liu, *Phys. Rev. Lett.* **72**, 3064 (1994).

¹⁰Q. Jiang, A. Chan, and G.-C. Wang, *Phys. Rev. B* **50**, 11 116

(1994); Q. Jiang and G.-C. Wang, *Surf. Sci.* **324**, 357 (1995).

¹¹H.-J. Ernst, F. Fabre, and J. Lapujoulade, *Phys. Rev. B* **46**, 1929 (1992).

¹²Y. Fujii, K. Narumi, K. Kimura, M. Mannami, T. Hashimoto, K. Ogawa, F. Ohtani, T. Yoshida, and M. Asari, *Appl. Phys. Lett.* **63**, 2070 (1993).

¹³R. Pfandzelter, *Nucl. Instrum. Methods Phys. Res. B* **157**, 291 (1999); *Phys. Rev. B* **57**, 15 496 (1998).

¹⁴R. Pfandzelter, T. Igel, and H. Winter, *Surf. Sci.* **389**, 317 (1997).

¹⁵J.-K. Zuo and J. F. Wendelken, *Phys. Rev. Lett.* **66**, 2227 (1991).

¹⁶M. C. Bartelt and J. W. Evans, *Surf. Sci.* **298**, 421 (1993).

¹⁷K. Morgenstern, G. Rosenfeld, and G. Comsa, *Phys. Rev. Lett.* **76**, 2113 (1996).

¹⁸N. C. Bartelt, W. Theis, and R. M. Tromp, *Phys. Rev. B* **54**, 11 741 (1996).

¹⁹J. B. Hannon, C. Klünker, M. Giesen, H. Ibach, N. C. Bartelt, and J. C. Hamilton, *Phys. Rev. Lett.* **79**, 2506 (1997).

²⁰P. M. DeLuca and S. A. Barnett, *Surf. Sci. Lett.* **426**, L407 (1999).